Analyst

Accepted Manuscript

This article can be cited before page numbers have been issued, to do this please use: H. Cui, S. Cui, S. Zhang, Q. Tian, Y. Liu, P. Zhang, M. Wang, J. Zhang and X. Li, *Analyst*, 2021, DOI: 10.1039/D1AN01323H.

DOI: 10.1039/D1AN01323H

Cu-MOFs/Hemin：A bionic enzyme with excellent dispersity for the determination of hydrogen peroxide released from living cells

Hong Cui*[a,1], Shuaishuai Cui[a,1], Siyuan Zhang[a], Qiuju Tian[a], Yunfeng Liu[a], Ping Zhang[a], Mingxiu Wang[a], Jialing Zhang[a] and Xiangjun Li*[b]

[a] *School of Public Health, Shanxi Medical University, 56Xinjian South Road, Taiyuan, 030001, China*

[b] *School of Chemical Sciences, University of Chinese Academy of Sciences, 19A Yuquan Road, Beijing, 100049, China*

* Corresponding authors. *E-mail addresses*: lixiangj@ucas.ac.cn (X. Li), cuihong19872007@126.com (H. Cui).

[1] co-first authors

View Article Online
DOI: 10.1039/D1AN01323H

Abstract

The stability, repeatability and sensitivity of an electrochemical biosensor material are closely connected with the dispersibility of metal organic frameworks (MOFs) in aqueous medium. Herein, a nanocomposite based on Cu-MOFs/Hemin, which is not only highly water-soluble but also simple and efficient in synthesis, was used for the construction of a non-enzymatic sensor to detect hydrogen peroxide (H_2O_2). The Cu-MOFs/Hemin was characterized via scanning electron microscopy (SEM), transmission electron microscopy (TEM), energy dispersive X-ray spectroscopy (EDS)-mapping, X-Ray diffraction (XRD), fourier transform infrared spectroscopy (FT-IR), X-ray photoelectron spectroscopy (XPS) and thermal gravity analysis (TGA), which indicate the hemin and Cu-MOFs were successfully combined. As a H_2O_2 electrochemical biomimetic enzyme, the Cu-MOFs/Hemin exhibited excellent electrocatalytic performance, which was confirmed by the electrochemical experiments and chromogenic reactions, as well as the possible mechanism of the reactions has been deduced. The electrochemical sensor based on the biomimetic enzyme exhibited an extended linear detection range from 0.01–5.0 mM (R=0.998), low detection of 4.14 μM, high selectivity and stability under the optimized conditions. More importantly, the practical application ability of the sensor was verified by the test of H_2O_2 in human serum samples and it could be used for the real-time detection of H_2O_2 released from living cells with satisfactory results. Therefore, this novel nanocomposite has the certain potential to prepare electrochemical sensing platform for nonenzymatic biosensing and provides a new method for clinical diagnosis and real-time monitoring.

Keywords: metal organic framework; hemin; non-enzymatic hydrogen peroxide sensor; human serum; living cells

View Article Online
DOI: 10.1039/D1AN01323H

1 Introduction

Hydrogen peroxide (H_2O_2), as a major member of reactive oxygen species (ROS) and the second messengers for cellular communications, is not only widely used in biopharmaceutical, chemical, environmental protection and many other fields, but also plays a significant role in intracellular signaling transduction, enzymatic reaction and internal environment stability of the body.[1-5] With the study of the body's internal environment, an increasing number of researchers have found that many chronic diseases and cell damage are directly or indirectly related to oxidative stress caused by the abnormal concentration of H_2O_2, such as Alzheimer's disease, Parkinson's disease, atherosclerosis, diabetes, and so on.[6-9] What's more, it was reported in the literature that the normal extracellular levels of H_2O_2 are found to be in the range of 0.001-0.1 μM, while the tumor cells produce higher concentrations of H_2O_2 (100 μM-1 mM) than normal cells due to the metabolism of tumor cells changes dramatically.[10,11] Therefore, changes in the concentration of H_2O_2 is closely related to human health and maybe an auxiliary factor for cancer accurate diagnosis.[12] For example, Wang et al. reported that H_2O_2 is a cofactor in the diagnosis of cervical cancer.[13] Hence, it is in dire need of exploiting an accurate and sensitive method to detect the H_2O_2 in human serum and living cells for early diagnosis of certain cancers and vascular diseases. Up to now, numerous analytical techniques and methods have been established to detect H_2O_2, such as titrimetry, spectrophotometry, fluorometry, chromatography, flow injection, chemiluminescence, and electrochemical methods.[14-18] Among these, electrochemical technology has the advantages of low detection limit, high sensitivity and selectivity, simple operation, low cost, as well as high convenience compared with other technologies. So electrochemical techniques have been widely used to detect H_2O_2 in real-time.[19] Early electrochemical sensing of H_2O_2 focused on the use of natural enzymes due to their high specificity and efficiency, but the enzyme-based H_2O_2 biosensors have some intrinsic weaknesses, which including rigorous demand on the experimental conditions, instability, easy

View Article Online
DOI: 10.1039/D1AN01323H

deactivation, and so on.[20,21] Therefore, it is very necessary to develop nanomaterial-based artificial and new-style enzymes with peroxidase mimics to replace the natural enzymes.

To the best of our knowledge, hemin (iron protoporphyrin IX) has attracted extensive attention of tremendous scientists because it is not only the active center of the heme-protein family including cytochromes, peroxidases, myoglobin, and hemoglobin, but also it can catalyze a lot of oxidation reactions like peroxidase enzymes.[22-25] Thus, many Hemin-based H_2O_2 biosensors have been fabricated in the last few years. For example, covalently binding of hemin to a gold electrode modified with the cystamine monolayer was reported.[26] Nevertheless, direct application of hemin as a catalyzer tends to suffer from poor catalytic activity and stability due to its oxidative self-degradation and the formation of inactive dimers by molecular aggregation in aqueous solution.[27,28] To overcome these drawbacks, hemin usually is used for the synthesis of MOFs as a ligand or needs to be immobilized onto a carrier with the high surface area such as metal/metal oxide nanostructures, silica, zeolites, polymer films, porous carbon and MOFs, where its catalytic activity could be effectively enhanced.[29-31] As one of the most promising immobilization carrier candidates in recent years, MOFs assembled from inorganic nodes and organic ligands have gained widespread attentions in the electrochemical fields such as supercapacitor, catalysis, and electrochemical sensors owing to their large internal surface areas, active and uniform metal sites, structural diversity, and remarkable adsorption ability.[32-35] For example, Qin and co-workers immobilized the hemin on the amino-containing MOF for preparing peroxidase mimicking catalysts and applied the functionality of MOFs for colorimetric detection of H_2O_2.[36] Wang and co-workers synthesized Cu-hemin MOFs/chitosan (CS)-reduced graphene oxide (CS-rGO) nanocomposite and applied it to the determination of H_2O_2 for the first time.[28] Combining the merits of MOFs and hemin, on the one hand, MOFs can effectively prevent the dimerization of the hemin molecule to improve the hemin performance; On the other hand, hemin and the active sites in the MOFs cooperate to promote the interfacial electron transfer and catalytic activity, showing the synergistic effect.[37]

View Article Online
DOI: 10.1039/D1AN01323H

However, the dispersion and film-forming properties of materials has always been an issue in electrochemical sensor due to the large size of synthetic materials, which would affect the reproducibility to a large extent. In order to overcome these shortcomings, CS or nafion was usually introduced to anchor the materials stably onto the electrodes to improve the film formation and dispersibility. Although the above problems are solved to a certain extent, the electron transfer capability will be compromised and the amounts of each modification of CS or nafion still affect reproducibility.

Herein, encouraged by the advantages of hemin and MOFs, a kind of Cu-MOFs using m-phthalic acid (PA) as organic ligand was synthesized via a simple hydrothermal route. As one of the typical carboxylic acids ligand, PA has been widely used in the synthesis of MOFs due to its abundant coordination patterns and the properties of multidimensional extension that attributed to the 120° separation between its two carboxylic groups. Some new structures of MOFs with PA as ligand could been easier to designed and prepared, and the easy channels functionalization of the synthetic MOFs gives the material some outstanding characteristics. Moreover, in recent years, PA has been transformed from the main ligand of the MOFs to the vacant structure-modulated ligand of the MOFs, which is mainly used for bridging, filling coordination positions and equalizing electric charges. PA can be used to link the mental center with other ligands through the double and single tooth or chelating dentate coordination pattern, then various two-dimensional plane structure or three-dimensional structure could be formed.[38-42] In this paper, the Cu-MOFs was firstly used as a novel immobilization matrix for hemin to fabricate a H_2O_2 biosensor. The electrode modification layer has good film-forming property without using the CS or nafion and exhibits favorable electrocatalytic activities towards the reduction of H_2O_2, which display high sensitivity, good stability and repeatability toward the reduction of H_2O_2. The schematic diagram of the synthetic routes of the materials and the construction of the electrochemical sensor is shown in Scheme 1. Besides, the catalase activity of this material was further investigated by TMB chromogenic reaction and a series of controlled tests. More

View Article Online
DOI: 10.1039/D1AN01323H

importantly, the fabricated Cu-MOFs/Hemin based sensor can be used for detecting H_2O_2 in human serum and the real-time tracking of H_2O_2 secreted by live cells.

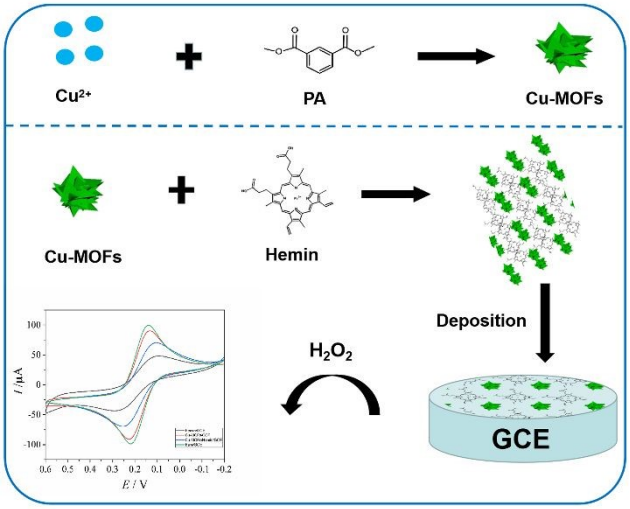

Scheme 1

2 Material and methods

2.1 Chemicals

$Cu(NO_3)_2 \cdot 3H_2O$ with purity of > 99.99%, Hemin with purity of > 95%, H_2O_2 (30%), uric acid (UA), ascorbic acid (AA), glucose (Glu), Glycine (Gly), Sodium chloride (NaCl), Potassium chloride (KCl), Dopamine hydrochloride (DA) were obtained from Aladdin Chemistry Co., Ltd (Shanghai, China). N, N-dimethylformamide (DMF, 99.5%) and m-phthalic acid (PA, 98%) were purchased from Roche. L-Lysine (L-Lys), L-Cysteine (L-Cys), L-Tyrosine (L-Tyr), L-Threonine (L-Thr) were obtained from Macklin Biochemical Co., Ltd (Shanghai, China). Catalase and phorbol 12-myristate 13-acetate (PMA) were purchased from Sigma-Aldrich. All the chemicals were used as received without further purification. Phosphate buffer solution (PBS, 0.1 M) was prepared by adjusting the volume ratios of the solution containing Na_2HPO_4 and NaH_2PO_4. Ultrapure water was used to prepare all aqueous solution throughout the experiments.

2.2 Apparatus

View Article Online
DOI: 10.1039/D1AN01323H

The surface structures, morphologies and element distribution information were acquired by using Energy dispersive X-ray spectroscopy (EDS) and field-emission scanning electron microscope (FE-SEM, SU8010, Hitachi) and transmission electron microscopy (TEM, JEM-2100, JEOL). X-ray powder diffraction (XRD) analysis was performed on a Bruker D8 Advance Diffractometer (Germany) with Cu Ka radiation to analyze the crystal structures of nanomaterials. The elemental composition and the functional groups of nanomaterials were analyzed by using X-ray photoelectron spectroscopy (XPS, Thermo escalab, 250Xi) and Fourier transform infrared spectrophotometer (FT-IR, Nicolet iS50). Thermogravimetric analysis (TGA) was conducted using a NETZSCH STA 449 F5/F3 Jupiter in the temperature range between 30 and 900 ℃ in presence of nitrogen. UV-vis absorption spectra were obtained by a TU-1901 UV-vis spectrometer.

All electrochemical measurements were carried out by a CHI660E electrochemical workstation (Shanghai Chenhua Instruments Co., China) in a conventional three-electrode electrochemical cell, including a modified GCE as working electrode, a saturated calomel electrode as the reference electrode and a platinum wire as the auxiliary electrode.

2.3 Synthesis of Cu-MOFs

Cu-MOFs were prepared using a traditional solvothermal method. Typically, 0.1160 g $Cu(NO_3)_2 \cdot 3H_2O$ was dissolved in water (12 mL), and then, 42 mL DMF was added into the above solution. After that, 12 mL of DMF solution of PA (0.0797 g) was added to the 54 mL $Cu(NO_3)_2 \cdot 3H_2O$ aqueous solution under stirring. After stirring for 20 min, the mixture was sealed in a Teflon-lined stainless-steel autoclave with a capacity of 100 mL, heated at 160 °C for 3 h, and then cooled to room temperature naturally. Next, the resulting precipitate was collected by centrifugation at 13000 rpm for 15 min. Subsequently we washed the precipitates with absolute ethanol and ultrapure water for three times, respectively. Finally, the sediment dried in a vacuum drying oven at 60 °C overnight and stored in a vial for further using.

View Article Online
DOI: 10.1039/D1AN01323H

2.4 Preparation of Cu-MOFs/Hemin nanocomposites

In a typical synthesis, the DMF solution (6 mL) of 10 mg Hemin was added to the 0.1 M NaOH solution (0.8 mL) and the mixture was sonicated for 30 min to obtain a complete homogeneous solution. Afterwards, 20 mg as-synthesized Cu-MOFs was added into the above mixed solution and continuously stirred for 30 min in magnetic stirrer (420 r). And then, the mixture solution was transferred to a Teflon-leaned autoclave with a capacity of 50 mL and heated at 100 °C for 24 h in an oven. After cooling the synthesis mixture to room temperature, the precipitate was collected by filtration, washed subsequently with DMF and ethanol for several times. Finally, the obtained black solid was dried under vacuum overnight and kept at 4 °C for further use. The different proportions of materials are obtained by the same procedure in the above description, while the different amounts of hemin (2, 5, 20, 30, 40 mg) were added in the starting synthesis system.

2.5 Fabrication of modified electrodes and electrochemical measurements

The glassy carbon electrode (GCE) was polished with 0.05 μm alumina powder followed by rinsing thoroughly with double distilled water, and then it was sonicated in ethanol and double distilled water successively for 1 min in order to obtain a mirror like electrode surface. Prior to using, the electrode was dried by N_2 gas purging. After that, 8 μL aqueous solution of Cu-MOFs/Hemin (3 mg/mL) was drop-coated on the surface of the well-polished GCE and dried under an incandescent lamp. After being dried, the electrode was used for electrochemical studies. In order to control, Hemin/GCE and Cu-MOFs/GCE were prepared in the similar procedure. In addition, all tests were carried out in a 0.1 M PBS passed through the nitrogen for 10 min to remove the oxygen at room temperature. Moreover, it's worth noting that the current signals were recorded in the chronoamperometric tests under magnetic stirring with increasing of H_2O_2 concentration.

2.6 Real sample analysis

2.6.1 H_2O_2 analysis in human serum samples

View Article Online
DOI: 10.1039/D1AN01323H

The human serum samples were collected from the Affiliated Hospital of Shanxi University of Chinese Medicine. In order to evaluate the practical application ability of the biosensors in real samples, we added different doses of H_2O_2 to the diluted serum and calculated the recovery. The procedure of the sample solutions for measuring is as follows: 20 μL serum and different concentrations of H_2O_2 were successively injected to the 10 mL 0.1 M PBS and all solutions need to be deoxidized through the nitrogen for 10 min. Then, the i-t curve was used to measure the current changes and the corresponding H_2O_2 concentration was calculated using the standard curve.

2.6.2 Measurements of the H_2O_2 released from cancer cells

Human hepatoma cancer (HepG2) cells were supplied by the Cell Bank of Chinese Academy of Sciences. HepG2 cells were grown in 75 cm^2 flasks in Dulbecco's modified Eagle medium containing 10% (v/v) fetal bovine serum and 1% penicillin/streptomycin at 37 °C in a 5% CO_2 environment. After reaching about 90% confluence, the media was eliminated and the cells were harvested by low-speed centrifugation and washed three times with PBS (0.1 M, pH=7.0). The cell number was estimated using a hemocytometer and the about 1.0×10^6 cells were suspended in 5 mL PBS (0.1 M, pH=7.0) deoxidized through the nitrogen for 10 min. Finally, the i-t curve was recorded to determine the content of H_2O_2 secreted from living cancer cells in real-time.

3 Results and discussion

3.1 Characterization of the Cu-MOFs/Hemin

SEM and TEM measurements were carried out to characterize the morphologies of Cu-MOFs and Cu-MOFs/Hemin nanocomposite. As shown in Fig. 1A and Fig. 1C, the SEM and TEM image of Cu-MOFs materials clearly indicate that the pure Cu-MOFs look like many octahedral diamonds stacked into 3D chrysanthemums-like shape and they are evenly dispersed in size about 2-4 μm. However, when hemin molecules were added to Cu-MOFs, the morphology of the complex is completely different from that of the pure Cu-MOFs. As can be seen from Fig. 1B and Fig. 1D, the obtained Cu-MOFs/Hemin nanocomposites present a

View Article Online
DOI: 10.1039/D1AN01323H

two-dimensional lamellar structure and the surface of which is very rough, indicating the hemin is involved in the coordination pattern of Cu-MOFs and it was successfully bonded on the Cu-MOFs. In addition, according to the element mapping results of O, C, Cu, N and Fe elements of the Cu-MOFs/Hemin nanocomposites in the EDS-mapping analysis, it can be seen that Fe elements were evenly distributed on the Cu-MOFs (Fig. S1A-F), which further confirmed the successful binding of Hemin molecule with Cu-MOFs. The XRD patterns of Cu-MOFs and Cu-MOFs/Hemin were essentially the same but intensity reduced where seems to be contradicted with the results of SEM (Fig. 2A), which could be explained that Cu-MOFs retained their original crystalline structure namely the coordination between Cu^{2+} and PA were not broken with the invasion of hemin but Cu-MOFs may directly coordinate with hemin and form large lamellar structures.

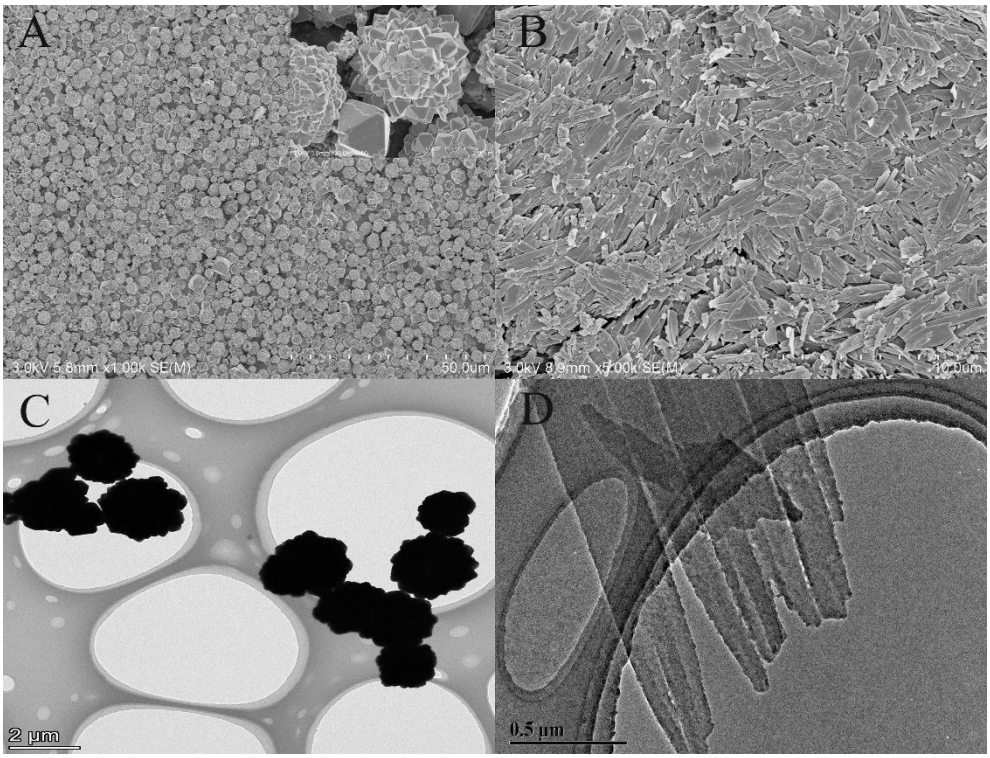

Fig. 1

FT-IR spectra were measured to identify the functional groups and types of chemical bond present in the Cu-MOFs/Hemin and Cu-MOFs (Fig. 2B), and the results observed in the spectrum are in accordance with previous literature reports.[36,43-46] The absorption peak around 3405 cm^{-1} in the FT-IR spectrum of

View Article Online
DOI: 10.1039/D1AN01323H

Cu-MOFs/Hemin powder is associated to the stretching vibration of O-H arising from the water molecules that exist on the surface of Cu-MOF/Hemin. Compared with Cu-MOFs, there are new strong peaks at 2914 cm^{-1} in Cu-MOFs/Hemin, which is assigned to stretching of the methyl functionalized group of hemin. The obvious absorption peaks that appear at approximately 1612 cm^{-1} and 1567 cm^{-1} can be ascribed to the stretching vibration of the C-O bond found in COO^-, which are arising from the asymmetric and symmetric vibrations of the C-O groups belonging to the carboxylate groups in Cu-MOFs. However, the peaks at these two locations are clearly red shifted in the curve of the Cu-MOFs/Hemin, indicating that the carboxyl group has been coordinated with the corresponding metal ions. Meanwhile, the absorption peak of Cu-MOFs at 1400-1550 cm^{-1} is the skeleton vibration of the benzene ring and the peaks ranging 950-700 cm^{-1} could be primarily assigned to the stretching vibration of the C-H benzene ring, respectively. Importantly, a new peak at 1119 cm^{-1} in Cu-MOFs/Hemin originated from C-N, proving the existence of hemin.

The XPS is a surface specific analytical tool that was carried out to qualitatively and quantitatively study the elemental composition, chemical state and electronic state of the corresponding elements that exist within material. The survey scanning full spectrum analysis result was shown in Fig. 2C in which five main elements including C, N, O, Fe and Cu can be comfortably distinguished in the Cu-MOFs/Hemin surface. High-resolution spectra of C1s, N1s, Cu2p, CuLM and Fe2p were present in Fig. S2, respectively. The high resolution XPS spectrum of C1s could be fitted into four peaks at banding energy around 284.6 eV, 284.9 eV, 286.6 eV, and 288.0 eV, illustrating the coexistence of the C-C, C=N, C-O-C and O-C=O, respectively. The diffraction peak observed at 398.2 eV in N1s region can be assigned to pyrrole nitrogen. The Cu2p high-resolution spectrum after fitting indicating that it can be divided into six typical characteristic peaks: Cu^+ $2p_{3/2}$ and Cu^+ $2p_{1/2}$ at 932.4 eV and 952.3 eV, Cu^{2+} $2p_{3/2}$ and Cu^{2+} $2p_{1/2}$ at 933.8 eV and 953.8 eV, while the peak at 941.4 eV and 944.2 eV are indexed to satellite peak. In addition, the Fe2p XPS spectrum of the Cu-MOFs/Hemin was analyzed and summarized. As can be seen, two pairs of

View Article Online
DOI: 10.1039/D1AN01323H

$2p_{3/2}/2p_{1/2}$ doublets for Fe^{2+} (710.2/723.1 eV) and Fe^{3+} (712.0/724.7 eV) and two satellite peaks located at 714.7 eV and 718.9 eV are deconvoluted for the Fe2p, suggesting the successful decoration of hemin in composite. Furthermore, the CuLM Auger peaks were performed to further determine the chemical valence state of copper and indicated that Cu^{+} is dominant in the complex.

In order to study the thermal stability, the TGA for Cu-MOFs/Hemin was subjected under N_2 atmosphere from room temperature to 900 °C at a heating rate of 10 °C min^{-1} (Fig. 2D). The Cu-MOFs curve shows a gradual weight loss of 3.5% at the temperature range of 30-300 °C corresponding to the removal of H_2O and other guest small molecules existing in interstitial spaces. With the further increase of temperature, the ligands of Cu-MOFs begin to decompose and the mass decreases sharply. The 63.9% of the mass of Cu-MOFs remains when the temperature rises to 900 ℃. But the complex begins to decompose at temperatures up to 170 °C, which most likely due to carbonization of the hemin in the complex and the decomposition of other small organic molecules in the pores. However, it can be seen from the curve in the figure that the change amount of the composite is slower than that of Cu-MOFs and the mass of the composite remains 68.9% when the temperature rises to 900 ℃, which indicates that the thermal stability of the composite material is improved.

View Article Online
DOI: 10.1039/D1AN01323H

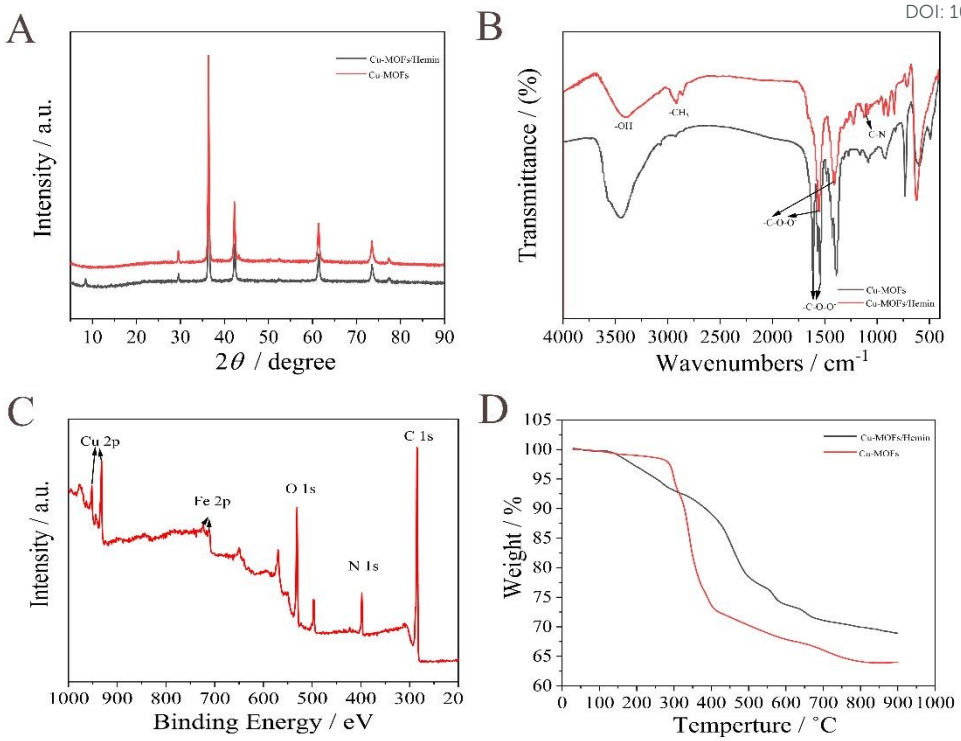

Fig. 2

3.2 Electrocatalytic behavior of modified electrode towards H_2O_2 reduction

The electrochemical impedance spectroscopy (EIS) technique was carried out to investigate electronic conductivity properties of different modified electrodes. A comparison of electrochemical impedance spectroscopy (EIS) curves for 5.0 mM $[Fe(CN)_6]^{3-/4-}$ in 0.1 mol L^{-1} KCl at bare, hemin modified, Cu-MOFs modified and Cu-MOFs/Hemin modified GCE were present in Fig. 3A. It can be clearly seen that the EISs of the electrodes show the order of semicircle diameter as follows (equal to the charge transfer resistance): Hemin/GCE>Cu-MOFs/Hemin/GCE> Cu-MOFs/GCE>bare GCE. That means, the electron transfer ability is Hemin/GCE<Cu-MOFs/Hemin/GCE<Cu-MOFs/GCE<GCE, which fully indicating the introduction of Cu-MOFs improve the electron transfer capability of hemin. These results are consistent with cyclic voltammetry (CV) measurements (Fig. 3B), in other words, the resistance of the electrode is inversely proportional to the current. This phenomenon is further illustrated that complex of the hemin and Cu-MOFs accelerate the electron transfer between analytes and electrodes.

View Article Online
DOI: 10.1039/D1AN01323H

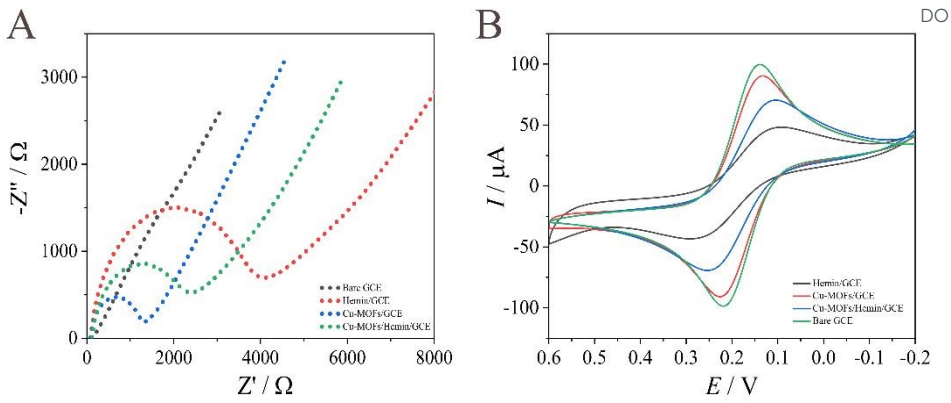

Fig. 3

In order to explore the application of the as-prepared Cu-MOFs/Hemin, we fabricated different electrochemical sensors of H_2O_2 using the Cu-MOFs, Hemin and Cu-MOFs/Hemin materials. The CVs of different modified electrode in 0.1 M PBS (pH=7.0) containing 0.3 mM H_2O_2 at a scan rate of 100 mV/s were shown in Fig. 4A. We can clearly see that there is no obvious redox peak of H_2O_2 at the bare GCE and only a slight redox peak current is observed at the Cu-MOFs/GCE in the potential range of -0.5 and 0.2 V, which indicate that Cu-MOFs has only a weak catalytic effect on H_2O_2. In contrast, Hemin/GCE and Cu-MOFs/Hemin/GCE exhibits remarkable reduction peaks, especially the peak current of Cu-MOFs/Hemin/GCE was the highest, indicating that it has the best electrocatalytic performance for H_2O_2. The most likely reason for this phenomenon is that the synergistic catalysis of Cu-MOFs as well as hemin and the carboxyl group on hemin was used to coordinate with metal center on Cu-MOFs, and hemin was uniformly loaded on its surface, thus avoiding hemin aggregation. In order to verify that the nano-composite material avoids the aggregation of hemin, the aqueous solution of nano-composite and hemin with the same concentration were prepared respectively. As can be seen from Fig. S3, hemin dissolved in water produced obvious agglomeration phenomenon and became more obvious after stored for 30 min. However, Cu-MOFs/Hemin was uniformly dispersed in aqueous solution without agglomeration. Furthermore, in order to verify again the electrocatalytic ability of the Cu-MOFs/Hemin/GCE to H_2O_2, different concentrations of H_2O_2 were measured by using typical CVs. As shown in Fig. 4B, the reduction peak current

View Article Online
DOI: 10.1039/D1AN01323H

increase with the concentration of H_2O_2 increasing from 0 to 1.0 mM. Thus, these results clearly demonstrate that the Cu-MOFs/Hemin possess excellent catalysis ability towards H_2O_2.

Besides, CVs of Cu-MOFs/Hemin/GCE were investigated at various scan rates in the presence of 0.1 M PBS (pH=7.0) with 0.3 mM H_2O_2 in order to get the kinetic information for the reduction of H_2O_2 and explore the reaction mechanism on the proposed electrode. As show in Fig. 4C, the currents of reduction peak are enhanced gradually with the increasing of scan rate and were proportional to the square root of scan rate with the correlation coefficient (R^2) of 0.999 within the range of scan rates from 10 to 800 mV s^{-1}, which show that the kinetics for H_2O_2 reduction is a typical behavior of a diffusion-controlled electrochemical process. On the other hand, since protons in the solution could participate in the redox reaction of H_2O_2, we investigated the effect of different pH of supporting electrolyte on the electrocatalytic performance via CV. As noticed in Fig. 4D, reduction peak potential shifts slightly towards the negative potential with increased pH from 4.0 to 9.0, which suggests that protons were directly involved in the electrode reaction. What's more, the good linear relationship is found between the peak potential (*E*p) and pH, and the linear equation is E_p (V) = -0.0403pH + 0.0035 (r=0.98). Obviously, the slope 0.0403 V pH^{-1} is close to the theoretical value 0.0590 V pH^{-1} at 25 ℃, which indicates that the redox process is a proton assisted mechanism and the number of electrons participating in the reduction of H_2O_2 is equal to the number of protons. Simultaneously, the real conditions of human body's internal environment pH are close to neutral. Thus, the pH value of supporting electrolyte was chosen to be 7.0, considering the sensitivity of H_2O_2 determination for all experiments. Based on the above results and referencing to the previous researches,[47-49] a simplified reaction mechanism of Cu-MOFs/Hemin/GCE electrocatalysis towards H_2O_2 could be presumed reasonably as follows:

$$2Cu(II) + 2e^- = 2Cu(I)$$

$$2Cu(I) + H_2O_2 + 2H^+ = 2Cu(II) + 2H_2O$$

View Article Online
DOI: 10.1039/D1AN01323H

$$2Fe(III) + 2e^- = 2Fe(II)$$

$$2Fe(II) + H_2O_2 + 2e^- = 2Fe(III) + 2H_2O$$

$$Cu(I) + Fe(III) \rightleftharpoons Cu(II) + Fe(II)$$

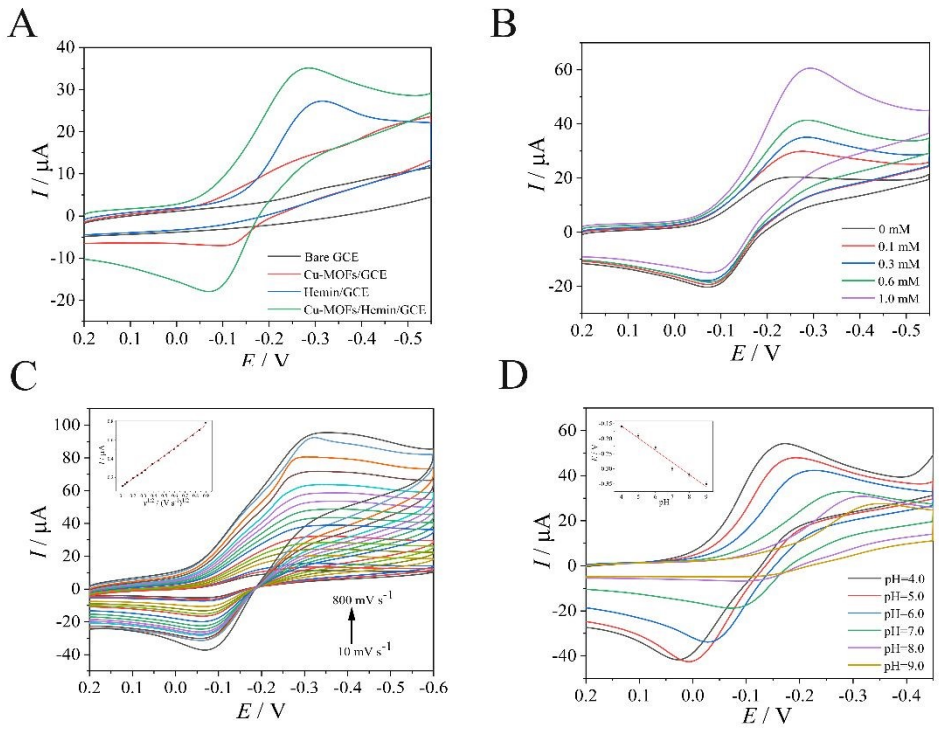

Fig. 4

In addition, suitable measures were taken to determine the optimum conditions before studying the typical amperometric response for H_2O_2. We optimized the ratio of hemin and the concentration of Cu-MOFs/Hemin for the best catalytic effect. Fig. S4A shows that the maximum current signal can be obtained when the mass ratio of hemin and Cu-MOFs was 1:2, thus we will use 10 mg hemin for the subsequent material synthesis without special version. The concentrations of Cu-MOFs/Hemin nanocomposite were optimized from 1 to 5 mg/mL by using CVs. It can be seen from the bar chart in Fig. S4B that the current responses increase with the enhancement of the concentrations of Cu-MOFs/Hemin, obtain the maximum value at 3 mg/mL and then decrease with the further increase of concentration, which may be attributed to the increasing exposure of active sites with the increase of concentration, but the higher the concentration, the more likely the material may fall off the electrode surface and

View Article Online
DOI: 10.1039/D1AN01323H

probably frustrated the catalytic capacity and reproducibility. Hence, the best concentration of the modified material was 3 mg/mL.

3.3 Amperometric performance of the H_2O_2 biosensor

Under the optimal experimental conditions, we used the amperometric method to evaluate the analytical performance of the Cu-MOFs/Hemin based biosensor towards the detection of H_2O_2. Fig. 5A displays the amperometric response of Cu-MOFs/Hemin/GCE with successive addition of H_2O_2 into the stirred 0.1 M PBS (pH=7.0) at the applied potential of -0.7 V. It was clearly found that the sensor responded quickly upon addition of H_2O_2 and achieved a steady-state level less than 4 s after each of the addition of H_2O_2, which demonstrated that obtained sensor had fast amperometric response for H_2O_2. The amperometric response was good linear relationship with H_2O_2 concentration from 0.01 to 5.0 mM with a detection limit of 4.14 μM, which was calculated based on the formula of $LOD = \frac{KS_b}{S}$ (K=3, S_b is the standard deviation of blank parallel determinations of 11 determinations, S is the sensitivity of the method) and the linear regression equation was I (μA) = 0.036957 c (mM) + 9.6486 (R^2=0.998) (Fig. 5B). Some other electrochemical sensors toward H_2O_2 detection were present in Table 1, and we can see that the Cu-MOFs/Hemin was compared with other non-enzyme H_2O_2 sensors and it possesses a low detection limit and a significantly wide linearity range, which may be attributed to the excellent electrocatalytic performance of composites.

Table 1

As is known to all, whether a new sensor can be widely used depends mainly on the following several critical factors including stability, repeatability, reproducibility, and the anti-interference ability. We also used the same modified electrode to continuously measure the same concentration of H_2O_2 in parallel for three times and three

View Article Online
DOI: 10.1039/D1AN01323H

different Cu-MOFs/Hemin modified electrodes were independently fabricated by the same way to measure H_2O_2 at the same concentration to obtain respective RSD of 4.12% and 4.01%, which suggested that the sensors based on the Cu-MOFs/Hemin/GCE have satisfied intra- and inter-electrode reproducibility and repeatability (Fig. S5A, S5B). In addition, the long-term stability of the Cu-MOFs/Hemin sensor was evaluated by comparing the response value of 0.3 mM H_2O_2 before and after five days at 4 °C in the refrigerator. The modified electrode still retained 90% of its initial current response, indicating well stability of the sensor (Fig. S5C). Furthermore, prior to the detection of real samples, the anti-interference ability of the material is also needing to be discussed, because the actual sample not only has H_2O_2 but also many other complex physiological interferences such as glycine, ascorbic acid, uric acid and other substances. What's more, the complex biological microenvironments are composed of thousands of metabolite molecules produced by a wide range of chemical reactions. Therefore, these possibly coexisting distractors were introduced to evaluate through the i-t curves. Fig. 5C shows the amperometric i-t curve for H_2O_2 at the Cu-MOFs/Hemin/GCE in 0.1 M N_2 saturated PBS (pH=7.0) containing several potential interferences. The current increased significantly when H_2O_2 was added at the beginning and at the end. However, no obvious responses could be seen at the Cu-MOFs/Hemin/GCE after addition the same concentration of glycine, ascorbic acid, uric acid, some amino acids in serum and other substances. These results revealed that the biosensor had excellent selective and remarkable specificity for H_2O_2 among these substrates, which mainly attributes to the properties of biomimetic enzymes with catalase and the size exclusion wherein H_2O_2 is smaller than the Cu-MOFs/Hemin's apertures could be adsorbed, but larger molecules such as AA and UA cannot be absorbed.

View Article Online
DOI: 10.1039/D1AN01323H

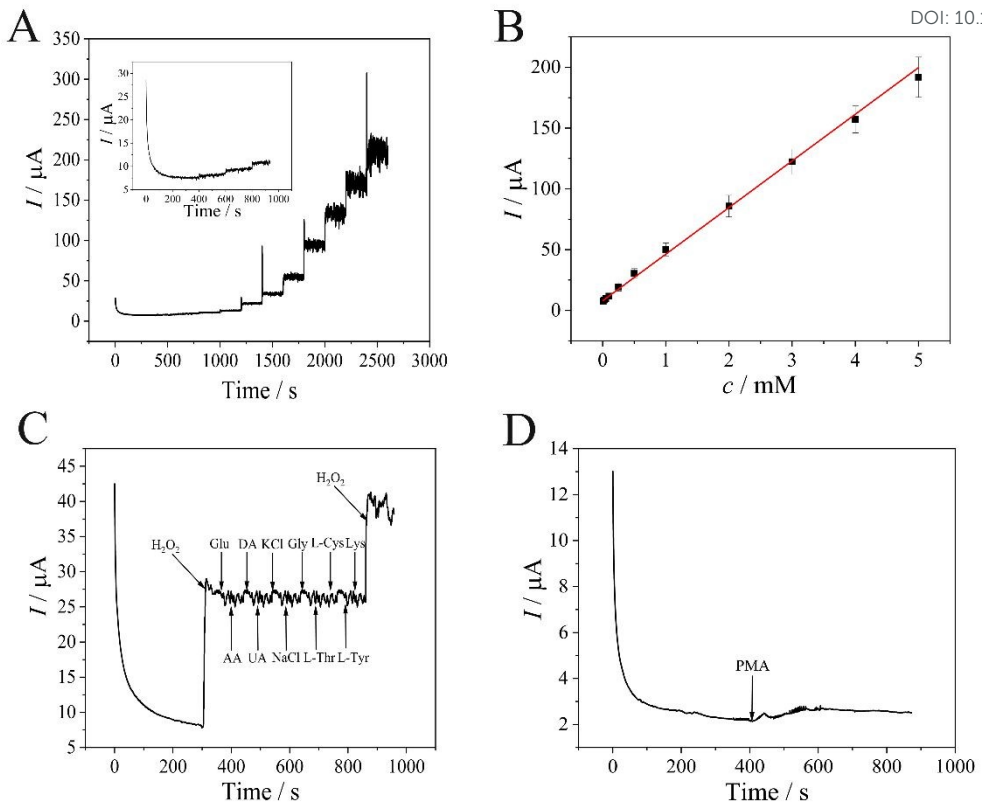

Fig. 5

3.4 Real sample analysis

The practical application of the proposed Cu-MOFs/Hemin/GCE was utilized by further measuring the concentration of H_2O_2 in human serum without any diseases and breast cancer patients. In total, three levels of standard solution were added to the serums for six parallel tests then by calculating the recovery to verify the feasibility of the method. The details are as follows: first, the samples were added to the deoxygenated 0.1 M N_2 saturated PBS (pH=7.0) after the current stabilized. Next, standard solutions of different concentrations were injected into the stirring PBS solution and measured by the i-t curve. Finally, the results were calculated and recorded in Table 2, we can see that the recoveries of H_2O_2 in the serum of normal people and cancer patient were in the range of 88.00%–110.00% and 98.47%–107.7%, and the corresponding of RSD were in the range of 2.90%–7.00% and 3.97%–8.70%, respectively.

View Article Online
DOI: 10.1039/D1AN01323H

Table 2

With the development of medical technology, more and more scientists have found that H_2O_2 holds a low concentration relatively under the normal physiological levels and the concentration of H_2O_2 in cancer cells is much higher than that in normal cells. Consequently, the biosensor fabricated was used to detect H_2O_2 released from HepG2 cells in real-time. Additionally, PMA was used as a stimulating agent and a proper amount of PMA can induce the H_2O_2 generation from living tumor cells within a short period of time.[50] It can be seen from the Fig. 5D that when 10 μL 10 μg mL^{-1} PMA was injected into the PBS medium containing HepG2 cells, an obvious change of current signal was obtained, which demonstrated that H_2O_2 can be released from HepG2 cells and catalyzed on the Cu-MOFs/Hemin/GCE in real-time. What's more, to further prove that the current was generated by the release of H_2O_2 from the cancer cells, we conducted a controlled experiment. In the control group, as a selective scavenger of H_2O_2, catalase (50 μL, 300 U mL^{-1}) was added to the cell culture medium prior to the addition of PAM, meanwhile the procedure was the same as in the experimental group. Interestingly, there was no measurable change of current response in the control group after the injection of PMA and the size of the current signal was almost identical to the background value (Fig. S6). Thus, the phenomenon further confirmed that H_2O_2 in the solution was indeed produced by cancer cells. By the above determination of the actual samples and cells, the proposed biosensor is capable of detecting H_2O_2 in real biological samples with high precisions and it is promising for the application of therapeutic strategies, cancer chemoprevention as well as physiological and pathological studies.

3.5 Peroxidase-like activity of the Cu-MOFs/Hemin material

In order to verify whether the Cu-MOFs/Hemin has peroxidase-like activity, we used chromogenic method by a UV-vis spectrophotometer and TMB was selected as the peroxidase chromogenic substrate. As shown in the inset

View Article Online
DOI: 10.1039/D1AN01323H

photo of Fig. 6, in the presence of different concentrations of H_2O_2, the Cu-MOFs/Hemin can catalytically oxidize TMB to give light green colors and the color deepens as the concentration of H_2O_2 increases. However, in the presence of the Cu-MOFs/Hemin or TMB alone, there were no obvious color reaction occurred, indicating the peroxidase-like activity of the hybrid material. It is worth mentioning that the light green color would be obvious in 5 min after the addition of the Cu-MOFs/Hemin, while only a little color change would occur with the addition of Cu-MOFs or Hemin.This explains that the catalytic activity of Cu-MOFs/Hemin is highest among the samples tested for the H_2O_2 reduction. Besides, we also measured the absorbance after the mixed solutions were incubated at room temperature for 5 min. Typically, the 3 mL buffer solution consisted of 10.2 μL of Cu-MOFs/Hemin material, 501 μL of TMB solution, H_2O_2 solution of different concentration and the final volume of the mixture were adjusted to 3 mL with 0.2 M acetate buffer (0.1 M, pH=4.0). As shown in the Fig. 6, there is an obvious absorption peak appeared at 652 nm and the absorbance increases with the increase of H_2O_2 concentration. However, the characteristic absorption peak was not generated in the absence of the Cu-MOFs/Hemin or TMB.

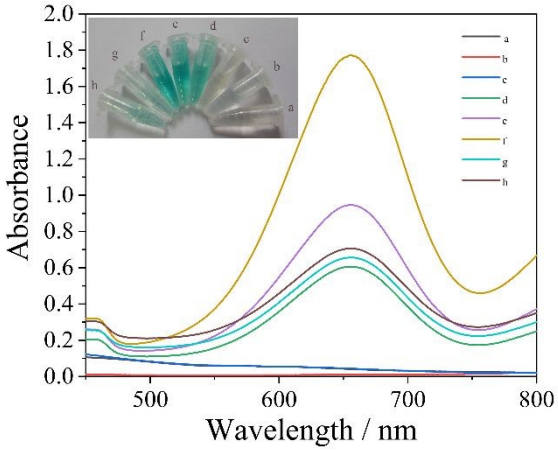

Fig. 6

4 Conclusion

In conclusion, an electrochemical sensor of H_2O_2 was successfully fabricated based on a bionic enzyme of the Cu-MOFs/Hemin nanocomposite with excellent water dispersibility. Cu-MOFs/Hemin could mimic inartificial

View Article Online
DOI: 10.1039/D1AN01323H

enzymes of high electrocatalytic activity for the H_2O_2, which could be attributed to the fact that the carboxyl group on hemin was used to coordinate with metal center on Cu-MOFs, and hemin was uniformly loaded on its surface, thus avoiding hemin aggregation as well as the synergistic catalysis of Cu-MOFs and hemin. The constructed biosensor based on the Cu-MOFs/Hemin nanocomposite showed good response toward H_2O_2 with a wide linear range from 0.01-5.0 mM, a low detection limit of 4.14 μM and satisfactory stability. What's more, our modified electrode not only measured H_2O_2 in the serum of normal people and cancer patients but also applied it to the determination of H_2O_2 at the cellular level, which confirmed the practical workability of the Cu-MOFs/Hemin nanocomposite based electrochemical sensor. Therefore, the results exhibit that the Cu-MOFs/Hemin will be a potential electrode material for the application in electroanalysis, and it might open up a new way to detect and monitor many other biologically and clinically crucial small molecules.

Author contributions

Hong Cui received her PhD degree of Analytical Chemistry from University of Chinese Academy of Sciences, Beijing, China in 2015. Since 2015 she is a lecture at Shanxi Medical University, China. Her main research interests focus on the design of composite materials based on metal-organic frameworks (MOF), biosensors, electroanalytical chemistry.

Shuaishuai Cui is currently pursuing his MS degree under the supervision of Dr. Hong Cui in Shanxi Medical University, China. His current research interests are mainly focused on the development and application of advanced materials, electroanalytical chemistry.

Siyuan Zhang is currently pursuing his MS degree under the supervision of Dr. Hong Cui in Shanxi Medical University, China. Her current research interests focus on the synthesis of nanomaterials and antimicrobial applications.

Qiuju Tian is currently pursuing his MS degree under the supervision of Dr. Hong Cui in Shanxi Medical

View Article Online
DOI: 10.1039/D1AN01323H

University, China. Her current research interests focus on the development of sample pretreatment methods.

Yunfeng Liu received her MS degree of Organic Chemistry from Nankai University, Tianjin, China in 2012. She is a lecture at Shanxi Medical University since 2013. Her major research interests focus on the design and synthesis of new type of porous organic materials and their application in sample pretreatment.

Ping Zhang received her Ph.D degree of Epidemiology and Health Statistics Biology from School of Public Health, Shanxi Medical University, China in 2018. Her research focus on the relations of environment and adverse birth outcomes.

Mingxiu Wang received her MS degree from Wuhan Institute of Virology, Chinese Academy of Sciences. She is a lecture at Shanxi Medical University since 2015. Her major research interests focus on the development and application of metal-organic frameworks (MOF)-based biosensors and cell imaging.

Jialing Zhang received her MS Degree in Analytical Chemistry from Shanxi University in 1996. She was as a visiting scholar at Juntendo University (Japan) in 2007. Currently, she is a professor in Shanxi Medical University, China. Her major interests of studies focused on the detection technology of toxic and harmful substances.

Xiangjun Li is currently a Professor in School of Chemical Sciences, University of Chinese Academy of Sciences. He received his MS Degree in 1999 from Shanxi University and his PhD Degree from Graduate University of Chinese Academy of Sciences in 2002. He was a postdoctoral researcher at Graduate University of Chinese Academy of Sciences from 2003 to 2006. He was as a visiting scholar at California state university in 2008. His current research emphasizes the molecular recognition, detection and chiral separation based on advanced materials, interactions between metal ions, small organic molecules and DNA or proteins, electroanalytical chemistry.

Compliance with ethical standards

All experiments were performed in accordance with the Guidelines of Shanxi Medical University (China) and

View Article Online
DOI: 10.1039/D1AN01323H

approved by the ethics committee at the Shanxi Medical University.

Conflicts of interest

There are no conflicts to declare.

Acknowledgements

This work was supported by the National Natural Science Foundation of China (No. 81803286), Science and Technology Innovation Project of Higher Education in Shanxi Province (No. 2020L0190), and the Natural Science Foundation of Shanxi Province (No. 201901D211328 and No. 201901D211326).

Notes and references

1 N. M. Jia, B. Z. Huang, L. Chen, L. Tan and S. Z. Yao, *Sens. Actuators B Chem.*, 2014, **195**, 165-170.

2 R. Z. Zhang and W. Chen, *Biosens. Bioelectron.*, 2017, **89**, 249-268.

3 S. Mutyala and J. Mathiyarasu, *Mater. Sci. Eng. C Mater. Biol. Appl.*, 2016, **69**, 398-406.

4 N. S. Lopa, M. M. Rahman, F. Ahmed, S. C. Sutradhar, T. Ryu and W. Kim, *Electrochim. Acta*, 2018, **274**, 49-56.

5 B. B Luo, X. M. Li, J. C. Yang, X. L. Li, L. P. Xue, X. L. Li, J. K. Gu, M. Z. Wang and L. Jiang, *Anal. Methods*, 2014, **6**, 1114-1120.

6 Z. H. Bai, G. Y. Li, J. T. Liang, J. Su, Y. Zhang, H. Z. Chen, Y. Huang, W. G. Sui and Y. X. Zhao, *Biosens. Bioelectron.*, 2016, **82**, 185-194.

7 B. Li, L. H. Liu, X. F. Zhang, Y. Gao, Z. P. Deng, L. H. Huo and S. Gao, *Electrochim. Acta*, 2021, **373**, 137908-137917.

8 H. Ohshima, M. Tatemichi and T. Sawa, Arch. *Biochem. Biophys.*, 2003, **417**, 3-11.

9 J. Liu, X. J. Bo, J. Yang, D. D. Yin and L. P. Guo, *Sens. Actuators B Chem.*, 2017, **248**, 207-213.

10 J. R. Stone and S. Yang, *Antioxid. Redox Sign.*, 2006, **8**, 243-270.

11 H. L. Tian, M. Z. Zhang, G. X. Jin, Y. Jiang and Y. X. Luan, *J. Colloid Interface Sci*., 2021, **587**, 358-366.

12 M. Hussain, A. Nisar, L. Z. Qian, S. Karim, M. Khan, Y. G. Liu, H. Y. Sun and M. Ahmad, *Nanotechnology*, 2021, **32**, 205501-205511.

13 L. Li, L. Ding, T. Gao, Y. J. Liu, M. Wang, L. Song, X. X. Li, W. Gao, Y. Han, H. X. Jia and J. T. Wang, *J. Cancer*, 2020, **11**, 284-291.

14 L. S. Zhang and G. T. F. Wong, *Talanta*, 1999, **48**, 1031-1038.

15 E. Kurowska-Tabor, K. Gawlak, K. Hnida, M. Jaskuła and G. D. Sulka, *Electrochim. Acta*, 2016, **213**, 811-821.

16 S. Chen, X. Hai, X. W. Chen and J. H. Wang, *Anal. Chem.*, 2014, **86**, 6689-6694.

17 P. Reanpang, S. Themsirimongkon, S. Saipanya, O. Chailapakul and J. Jakmunee, *Talanta*, 2015, **144**, 868-874.

18 N. V. Klassen, D. Marchlngton and H. C. E. McGowan, *Anal. Chem.*, 1994, **66**, 2921-2925.

19 H. X. Dai, W. J. Lu, X. W. Zuo, Q. Zhu, C. J. Pan, X. Y. Niu, J. J. Liu, H. L. Chen and X. G. Chen, *Biosens. Bioelectron.*, 2017, **95**, 131-137.

20 Y. J. Sun, M. C. Luo, X. X. Meng, J. Xiang, L. Wang, Q. S. Ren and S. J. Guo, *Anal. Chem.*, 2017, **89**, 3761-3767.

21 P. Das, M. Das, S. R. Chinnadayyala, I. M. Singha and P. Goswami, *Biosens. Bioelectron.*, 2016, **79**, 386-397.

22 Y. J. Guo, L. Deng, J. Li, S. J. Guo, E. K. Wang and S. J. Dong, *ACS Nano*, 2011, **5**, 1282-1290.

23 S. B. Xie, J. W. Ye, Y. L. Yuan, Y. Q. Chai and R. Yuan, *Nanoscale*, 2015, **7**, 18232-18238.

24 E. Monzani, G. Alzuet, L. Casella, C. Redaelli, C. Bassani, A. M. Sanangelantoni, M. Gullotti, L. D. Gioia, L. Santagostini, and F. Chillemi, *Biochemistry*, 2000, **39**, 9571-9582.

25 M. M. Vdovenko, A. S. Demiyanova, K. E. Kopylov and I. Y. Sakharov, *Talanta*, 2014, **125**, 361-365.

View Article Online
DOI: 10.1039/D1AN01323H

26 T. L6tzbeyer, W. Schuhmann and H. L. Schmidt, *J. Electroanal. Chem.*, 1995, **395**, 341-344.

27 Y. Zang, J. P. Lei, L. Zhang and H. X. Ju, *Anal. Chem.*, 2014, **86**, 12362-12368.

28 L. Wang, H. Yang, J. He, Y. Y. Zhang, J. Yu and Y. H. Song, *Electrochim. Acta*, 2016, **213**, 691-697.

29 B. L. Li, H. Q. Luo, J. L. Lei and N. B. Li, *RSC Adv.*, 2014, **4**, 24256-24262.

30 C. Q. Li, W. G. Qiu, W. Long, F. Deng, G. M. Bai, G. Z. Zhang, X. H. Zi and H. He, *J. Mol. Catal. A: Chem.*, 2014, **393**, 166-170.

31 F. Q. Luo, Y. L. Lin, L. Y. Zheng, X. M. Lin and Y. W. Chi, *ACS Appl. Mater. Interfaces*, 2015, **7**, 11322-11329.

32 Y. Shu, Y. Yan, J. Y. Chen, Q. Xu, H. Pang and X. Y. Hu, *ACS Appl. Mater. Interfaces*, 2017, **9**, 22342-22349.

33 C. Qu, Y. Jiao, B. Zhao, D. C. Chen, R. Q. Zou, K. S. Walton and M. L. Liu, *Nano Energy*, 2016, **26**, 66-73.

34 A. Dhakshinamoorthy, A. M. Asiri and H. Garcia, *Chem. Commun.*, 2014, **50**, 12800-12814.

35 M. X. Wu and Y. W. Yang, *Adv. Mater.*, 2017, **29**, 1606134-1606153.

36 F. X. Qin, S. Y. Jia, F. F. Wang, S. H. Wu, J. Song and Y. Liu, *Cata. Sci. Technology*, 2013, **3**, 2761-2768.

37 H. Y. Shen, P. J. Sun, X. Meng, J. L. Wang, H. Y. Liu and L. J. Xu, *Chemosphere*, 2021, **269**, 128763-128773.

38 F. Luo, M. S. Wang, M. B. Luo, G. M. Sun, Y. M. Song, P. X. Li and G. C. Guo, *Chem. Commun.*, 2012, **48**, 5989-5991.

39 J. X. Chen, J. J. Wang and M. Ohba, *J. Solid State Chem.*, 2012, **185**, 37-41.

40 L. Wang and L. Ni, *J. Coord. Chem.*, 2012, **65**, 1475-1484.

41 S. X. Yan, D. Zhao, T. Li, R. Wang and X. R. Meng, *J. Coord. Chem.*, 2012, **65**, 945-957.

42 X. Z. Song, S. Y. Song, C. Qin, S. Q. Su, S. N. Zhao, M. Zhu, Z. M. Hao and H. J. Zhang, *Cryst. Growth*

View Article Online
DOI: 10.1039/D1AN01323H

Des., 2012, **12**, 253−263.

43 D. C. Cheng, X. Li, Y. Qiu, Q. Chen, J. Zhou, Y. Q. Yang, Z. Z. Xie, P. Liu, W. Q. Cai and C. C. Zhang, *Anal. Methods*, 2017, **9**, 2082-2088.

44 P. Gao, X. Y. Sun, B. Liu, H. T. Lian, X. Q. Liu and J. S. Shen, *J. Mater. Chem. C*, 2018, **6**, 8105-8114.

45 F. F. Liu, J. He, M. L. Zeng, J. Hao, Q. H. Guo, Y. H. Song and L. Wang, *J. Nanopart. Res.*, 2016, **18**, 1-9.

46 Q. J. Liu, Z. Y. He, H. Wang, X. Y. Feng and P. Han, *Microchim. Acta*, 2020, **187**, 524-532.

47 K. Karami, P. Bayat, H. Khosropour, F. Siadatnasab, B. Rezaei and A. Mardaniboldaji, *J. Electrochem. Soc.*, 2021, **168**, 017508-017516.

48 Y. Cao, W. M. Si, Q. L. Hao, Z. F. Li, W. Lei, X. F. Xia, J. Li, F. G. Wang and Y. Y. Liu, *Electrochim. Acta*, 2018, **261**, 206-213.

49 J. P. Ma, W. S. Bai and J. B. Zheng, *Microchim. Acta*, 2019, **186**, 482-489.

50 S. K. Maji, S. Sreejith, A. K. Mandal, X. Ma and Y. Zhao, *ACS Appl. Mater. Interfaces*, 2014, **6**, 13648-13656.

51 W. Liu, K. Hiekel, R. Hübner, H. J. Sun, A. Ferancova and M. Sillanpää, *Sens. Actuators B Chem.*, 2018, **255**, 1325-1334.

52 L. Z. Yang, C. L. Xu, W. C. Ye and W. S. Liu, *Sens. Actuators B Chem.*, 2015, **215**, 489-496.

53 J. X. Zhou, L. N. Tang, F. Yang, F. X. Liang, H. Wang, Y. T. Li, and G. J. Zhang, *Analyst*, 2017, **142**, 4322-4329.

54 D. J. Zhang, J. C. Zhang, R. C. Zhang, H. Z. Shi, Y. Y. Guo, X. L. Guo, S. J. Li and B. Q. Yuan, *Talanta*, 2015, **144**, 1176-1181.

55 T. Zhang, B. H. Zheng, L. Y. Song, L. Song and M. D. Zhang, *Appl. Surf. Sci.*, 2021, **539**, 148255-148260.

56 H. L. Liu, Y. Y. Cui, P. Li, Y. M. Zhou, X. S. Zhu, Y. W. Tang, Y. Chen and T. H. Lu, *Analyst*, 2013, **138**,

View Article Online
DOI: 10.1039/D1AN01323H

2647-2653.

57 J. Chen, B. B. Huang, S. Z. Zhan and J. S. Ye, *J. Electroanal. Chem.*, 2015, **759**, 194-200.

58 C. F. Cheng, C. M. Zhang, X. H. Gao, Z. H. Zhuang, C. Du and W. Chen, *Anal. Chem.*, 2018, **90**, 1983−1991.

Figure Captions:

Scheme 1. Schematic presentation for the fabrication of Cu-MOFs/Hemin/GCE and its application for the determination of H_2O_2.

Fig. 1. SEM images of Cu-MOF (A), Cu-MOFs/Hemin (B); TEM images of Cu-MOFs (C), Cu-MOFs/Hemin (D).

Fig. 2. (A) XRD of the Cu-MOFs and Cu-MOFs/Hemin. (B) FT-IR spectra of Cu-MOFs and Cu-MOFs/Hemin. (C) The XPS survey spectrum of Cu-MOFs/Hemin. (D) TGA curves of the Cu-MOFs and Cu-MOFs/Hemin under nitrogen atmosphere.

Fig. 3. (A) EIS images for bare GCE, Cu-MOFs/GCE, Hemin/GCE and Cu-MOFs/Hemin/GCE in 5 mM $[Fe(CN)_6]^{3-/4-}$ containing 0.1 M KCl at scanning frequencies from 0.01 to 100,000 Hz. (B) CV curves of bare GCE, Cu-MOFs/GCE, Hemin/GCE and Cu-MOFs/Hemin/GCE in 5 mM $[Fe(CN)_6]^{3-/4-}$ containing 0.1 M KCl at -0.2–0.6 V.

Fig. 4. (A) CV curves of bare GCE, Cu-MOFs/GCE, Hemin/GCE and Cu-MOFs/Hemin/GCE in N_2 saturated 0.1 M PBS (pH=7.0) in presence of 0.3 mM H_2O_2 at a scan rate of 100 mV s^{-1}. (B) CV curves of Cu-MOFs/Hemin/GCE in presence of different concentrations of H_2O_2 at a scan rate of 100 mV s^{-1}. (C) CV curves of MOFs/Hemin/GCE in presence of 0.3 mM H_2O_2 at different scan rates (10–800 mV s^{-1}). Inset: the corresponding calibration plots of currents for reduction and oxidation peak with the scan rates. (D) CVs of the Cu-MOFs/Hemin/GCE in an N_2 saturated 0.1 M PBS at different pH values. Scan rate: 100 mV s^{-1}. Inset: plot of the redox peak potential versus pH value.

View Article Online
DOI: 10.1039/D1AN01323H

Fig. 5. (A) i-t response of the Cu-MOFs/Hemin/GCE with successive addition of different concentration of H_2O_2 at the potential of -0.7 V. Inset: a partial magnification of the current response toward a low concentration of H_2O_2 (0–1000 s). (B) The corresponding calibration curve for H_2O_2 sensing. (C) i-t response curve of Cu-MOFs/Hemin upon successive addition of H_2O_2, Glu, AA, DA, UA, KCl, NaCl, Gly, L-Thr, LCys, L-Tyr and Lys in 0.1 M PBS at -0.7 V. (D) Typical amperometric responses of the Cu-MOFs/Hemin/GCE for the reduction of H_2O_2 release from HepG2 cells induced by PMA.

Fig. 6. The absorption spectra and digital photos of different reaction system in 0.1 M HAc-NaAc (pH=4.0): a: H_2O_2 + Cu-MOFs/Hemin, b: TMB + H_2O_2, c: 0 mM H_2O_2 + TMB + Cu-MOFs/Hemin, d: 0.5 mM H_2O_2 + TMB + Cu-MOFs/Hemin, e: 1 mM H_2O_2 + TMB + Cu-MOFs/Hemin, f: 2 mM H_2O_2 + TMB + Cu-MOFs/Hemin, g: 1 mM H_2O_2 + TMB + Cu-MOFs, h: 1 mM H_2O_2 + TMB + Hemin.

Table 1. Comparison of different MOFs and other nanomaterials based biosensors for H_2O_2 detection in terms of linear range and LOD.

Electrode materials	Linear range (μM)	LOD (μM)	Reference
SiO_2/APTMS[a] /AuPt	5.0-72000	2.6	51
$[Co(pbda)(4,4\text{-bpy})(2H_2O)]_n$	50-9000	3.76	52
MoS_2/Pt NPs	1-100	0.686	53
Cu-MOF	1-400	1.0	54
$[Co_3(HOB)_2]_n$ nanosheets	–	0.00308	55
EDTMP/Fe^{III}-DETPA/PAH-MWCNTs/Au	0.0125-4750	0.0063	56
Cu complex Au film	0.05-60	0.042	57
2D Cu_2O-rGO-P	5–10560	3.78	58
Cu-MOF/Hemin	10-5000	4.14	This work

View Article Online
DOI: 10.1039/D1AN01323H

Table 2. Analytical results for the determination of H_2O_2 in human serum samples.

Sample	Found (mM)	Added (mM)	After added (mM)	RSD (%)	Recovery (%)
		0.01	0.011	7.00	110.00
normal	0.00	0.05	0.044	2.90	88.00
serum		0.10	0.097	4.68	97.00
breast cancer		0.01	0.0098	3.97	98.47
patients'	0.11	0.05	0.051	8.70	103.8
serum		0.25	0.26	4.48	107.7